nature materials

Supplementary information

https://doi.org/10.1038/s41563-024-02023-7

Obtaining $V_2(PO_4)_3$ by sodium extraction from single-phase $Na_xV_2(PO_4)_3$ ($1 < x < 3$) positive electrode materials

In the format provided by the authors and unedited

Reaching $V_2(PO_4)_3$ by Sodium Extraction from Single-Phase $Na_xV_2(PO_4)_3$ ($1 < x < 3$) Positive Electrode Materials

Supplementary Information

Table of Contents

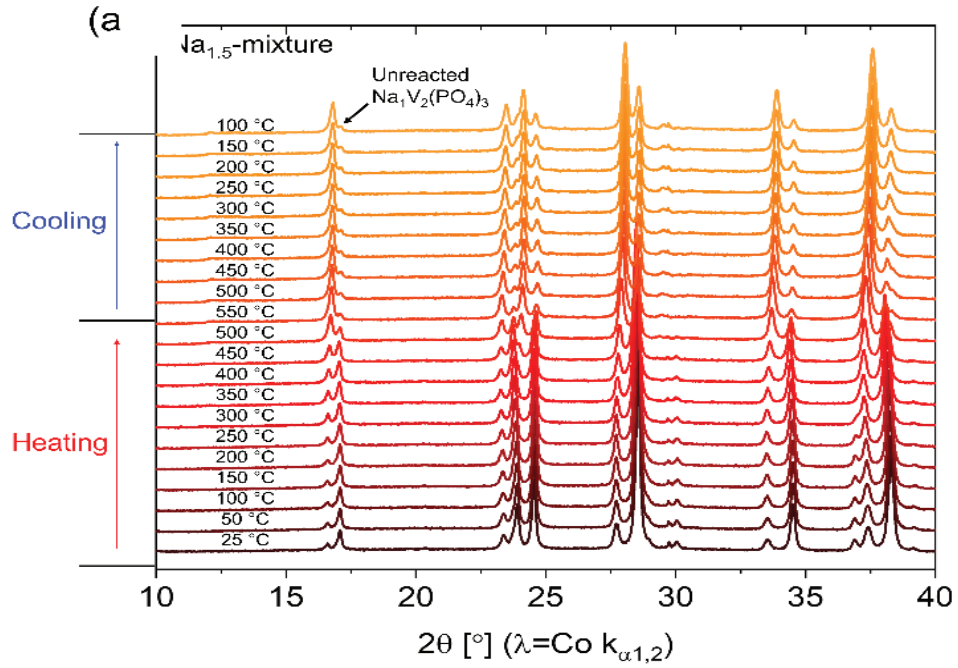

Figure S1a. Temperature-controlled *in situ* XRD patterns of the mixture of 0.25 $Na_3V_2(PO_4)_3$ and 0.75 $Na_1V_2(PO_4)_3$ collected every 50 °C upon heating up to 550 °C then cooling down to 100 °C.

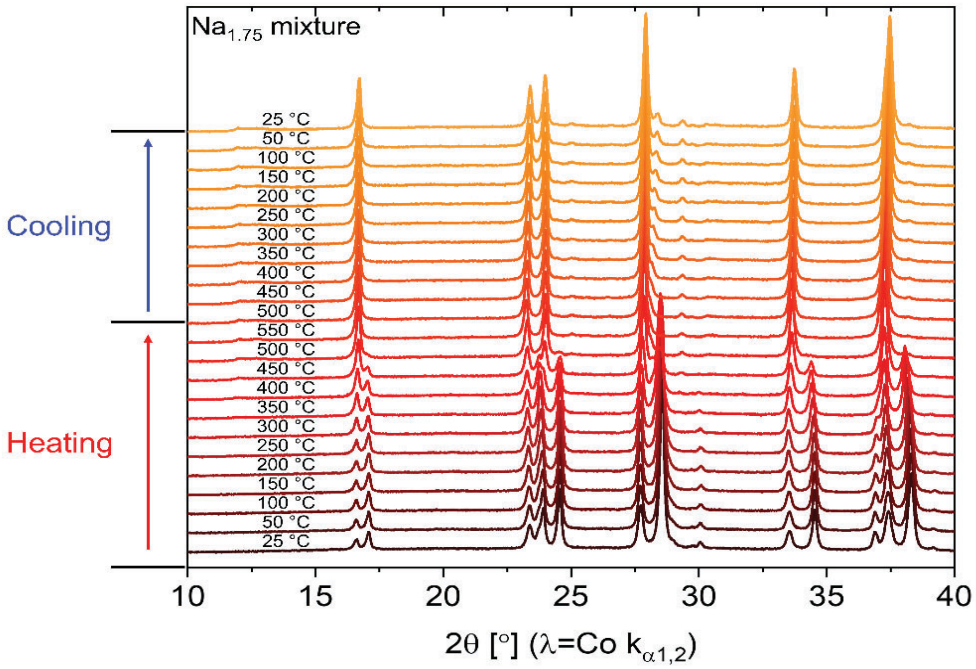

Figure S1b. Temperature-controlled *in situ* XRD patterns for the mixture of 0.375 $Na_3V_2(PO_4)_3$ and 0.625 $Na_1V_2(PO_4)_3$ collected every 50 °C upon heating up to 550 °C then cooling down to 25 °C.

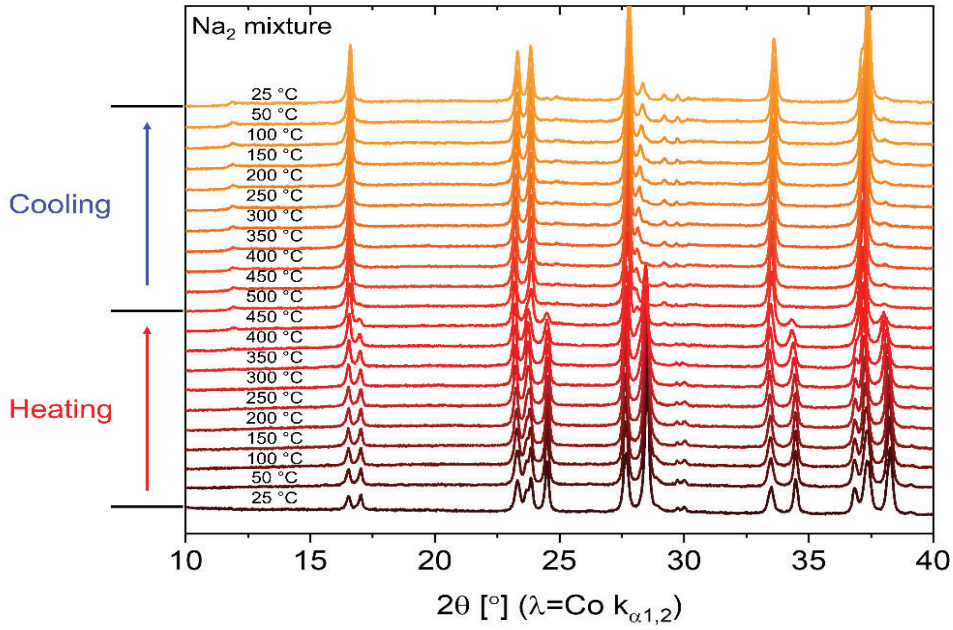

Figure S1c. Temperature-controlled *in situ* XRD patterns for the mixture of 0.5 $Na_3V_2(PO_4)_3$ and 0.5 $Na_1V_2(PO_4)_3$ collected every 50 °C upon heating up to 500 °C then cooling down to 25 °C.

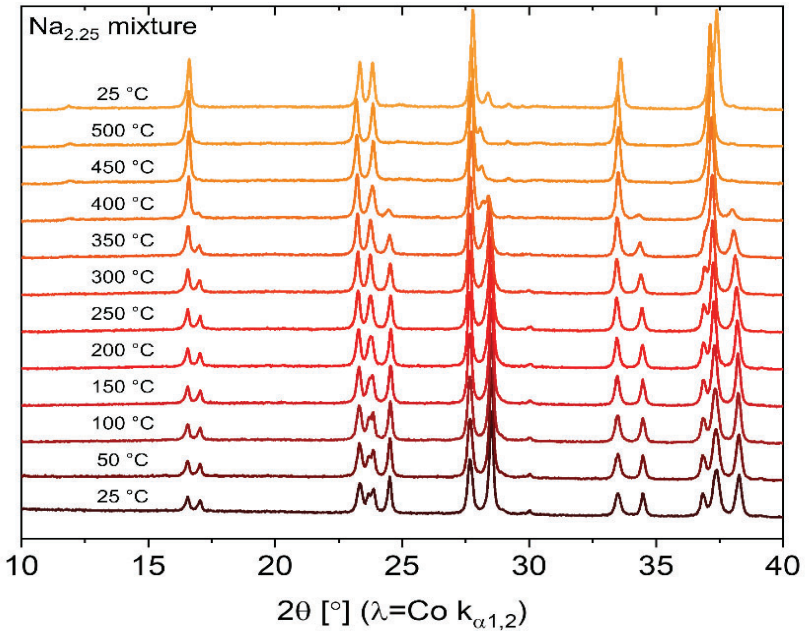

Figure S1d. Temperature-controlled *in situ* XRD patterns for the mixture of 0.625 $Na_3V_2(PO_4)_3$ and 0.375 $Na_1V_2(PO_4)_3$ collected every 50 °C upon heating up to 500 °C then measured at 25 °C after cool down.

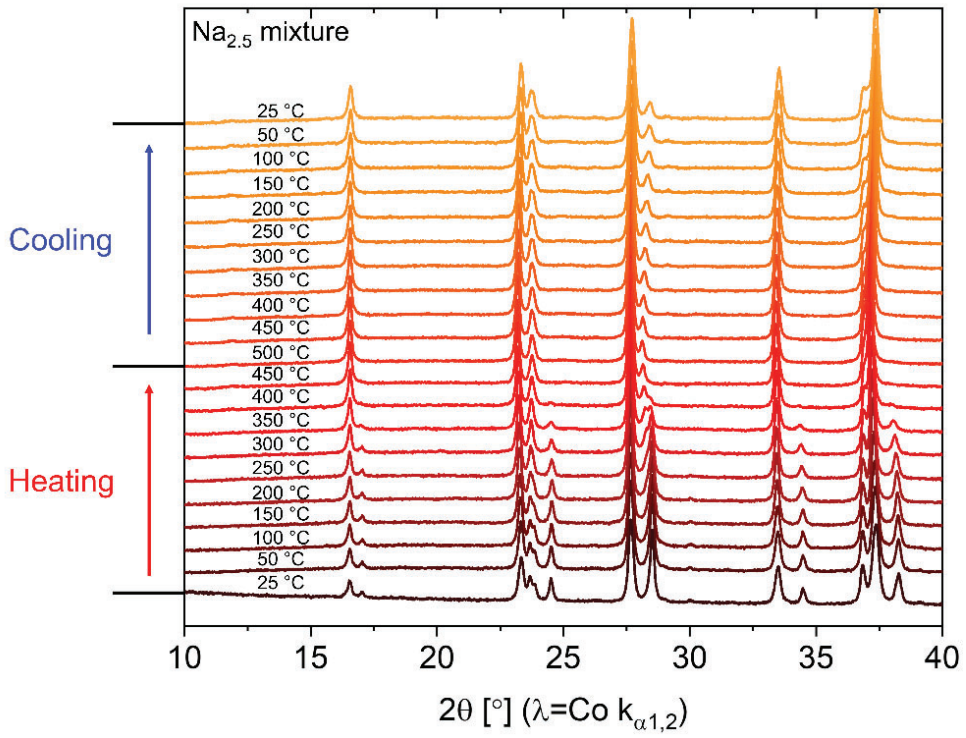

Figure S1e. Temperature-controlled *in situ* XRD patterns for the mixture of 0.75 $Na_3V_2(PO_4)_3$ and 0.25 $Na_1V_2(PO_4)_3$ collected every 50 °C upon heating up to 500 °C then cooling down to 25 °C.

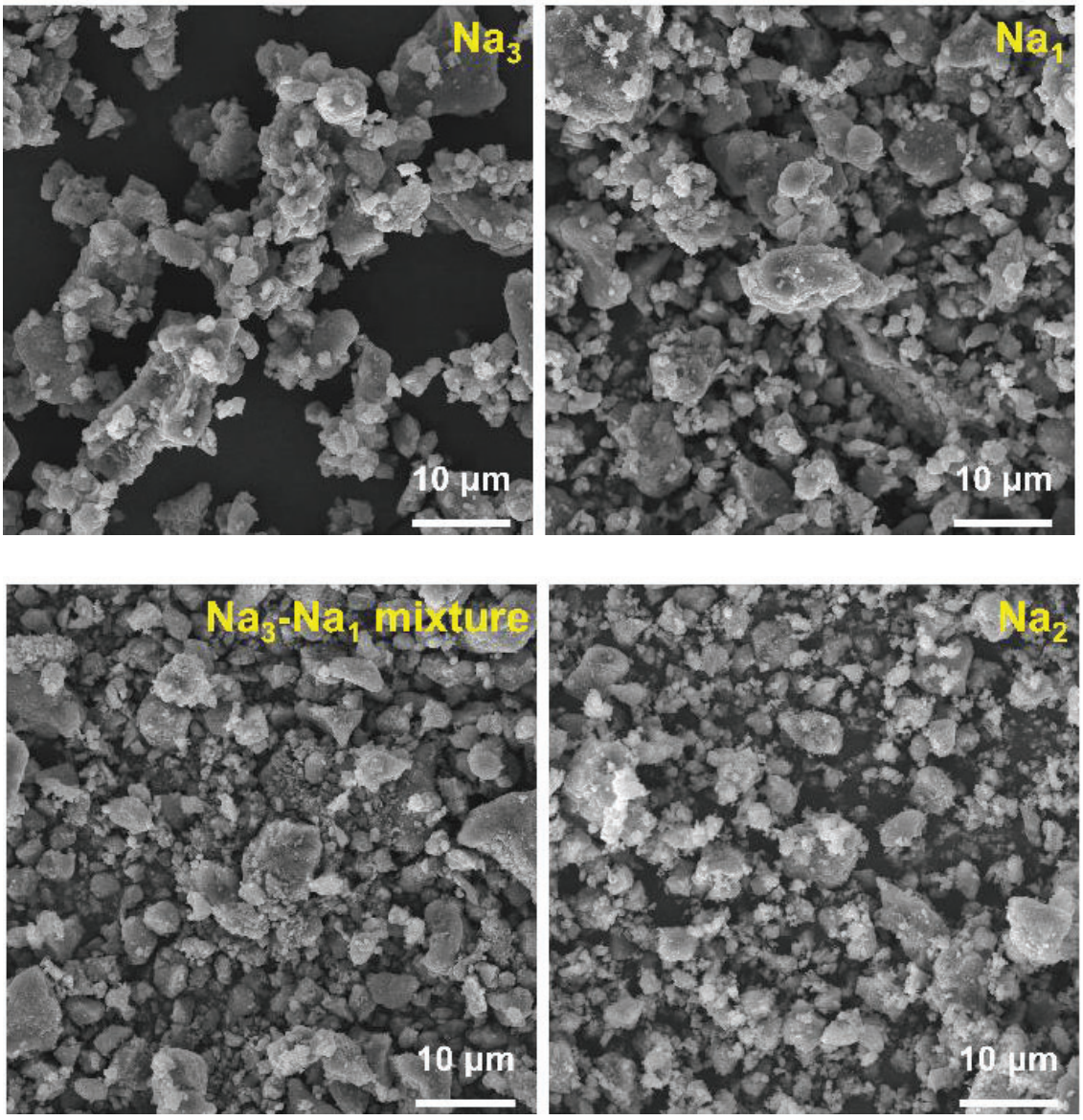

Figure S2. SEM images of $Na_3V_2(PO_4)_3$ (Na_3), $Na_1V_2(PO_4)_3$ (Na_1), mixture of $Na_3V_2(PO_4)_3$ and $Na_1V_2(PO_4)_3$ (Na_3-Na_1 1), and $Na_2V_2(PO_4)_3$ after annealing at 500 °C (Na_2).

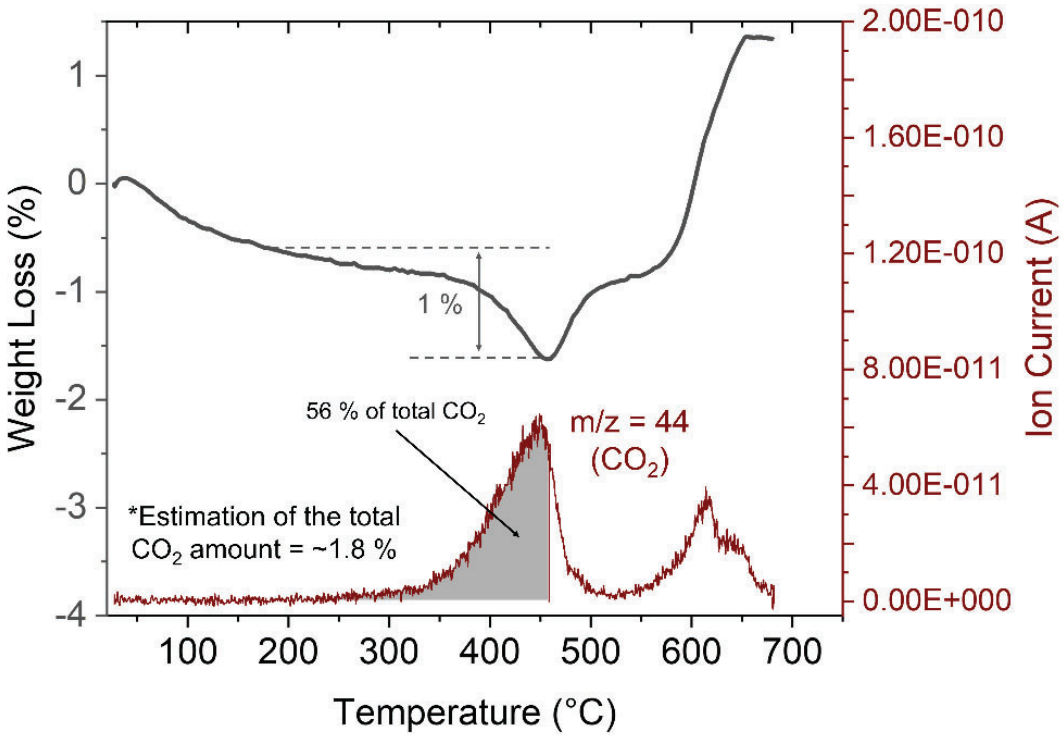

Figure S3. Thermogravimetric analysis, under air, combined with mass spectroscopy for the pristine c-$Na_3V_2(PO_4)_3$.

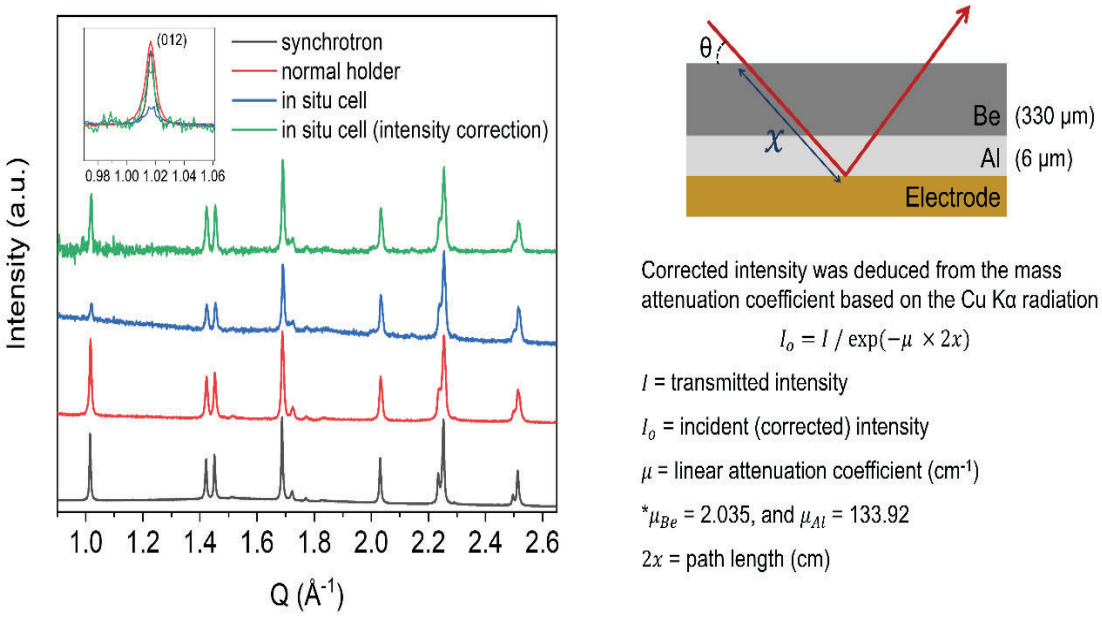

Figure S4: Comparison of the XRD patterns of the chemically-prepared $Na_2V_2(PO_4)_3$ obtained within synchrotron X-ray, lab X-ray with normal holder, lab X-ray with an *in situ* cell, and lab X-ray with an *in situ* cell after the intensity correction (mass attenuation coefficient).

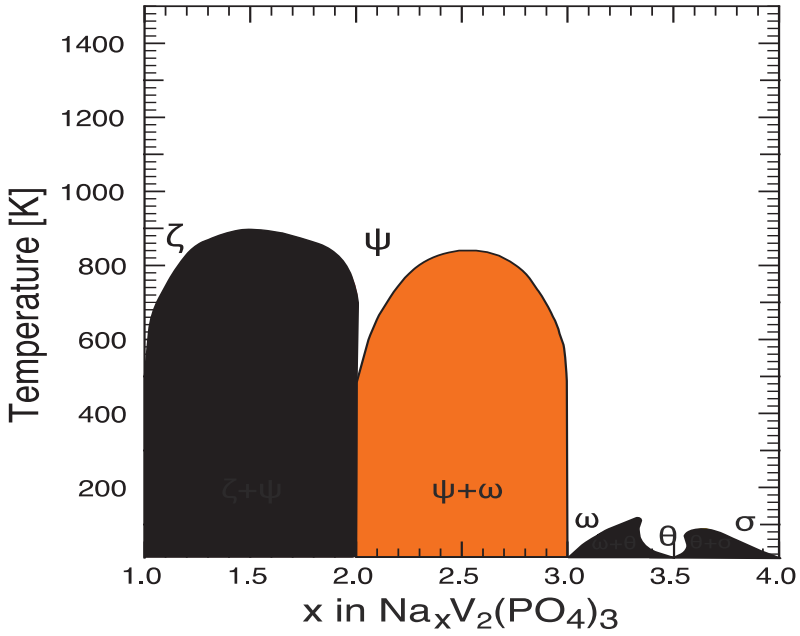

Figure S5. Predicted phase diagram of $Na_xV_2(PO_4)_3$ at variable Na contents (x) and temperatures (T). Solid lines show the phase boundaries. Precisely, ζ, ψ, and ω correspond to single-phase regions at Na compositions of x = 1, 2 and 3, respectively. At 0 K, ζ, ψ, and ω exist as the stable phases and have the same Na(1) / Na(2) occupations as the e-GS phases shown in **Table 2** of the main manuscript. Reproduced from Ref. [1] with permission from the Royal Society of Chemistry.[1]

The phase diagram of **Figure S2,** above, justifies the stability region of all single phases. For example, Na_2VP phase is stable and thermodynamically preserved over wide temperature region (i.e., 0 – 800 K). Additionally, the derived configurational entropy S(x) in Ref. [1] also shows a local minimum at x = 1, 2, and 3, respectively, which agrees with the appearance of single phases ζ, ψ, and ω in this work. Notably, S(x) in Ref. 16 indicates all the derived single phases (i.e., ζ, ψ, and ω) are line compounds. All these results emphasize the formation of a single phase at RT. By the experimental procedure highlighted in this work (mixing and then annealing), we can further identify additional single phases, such as $Na_{1.5}VP$, $Na_{1.75}VP$, $Na_{2.25}VP$ and $Na_{2.5}VP$, which compensate for the formation of line compounds being stable at room temperature.

Density of States of $Na_1V_2(PO_4)_3$

Figure S6 and **Figure S7** show the computed density of states (DOS) for different phases of $Na_1V_2(PO_4)_3$ (see **Table 1** of main text), i.e., the electrochemically-ground-state with fully occupied Na(1) (e-GS), metastable-α with Na(1)-occ of 0.75, metastable-β with Na(1)-occ of 0.5 and metastable-γ with Na(1)-occ of 0.25.

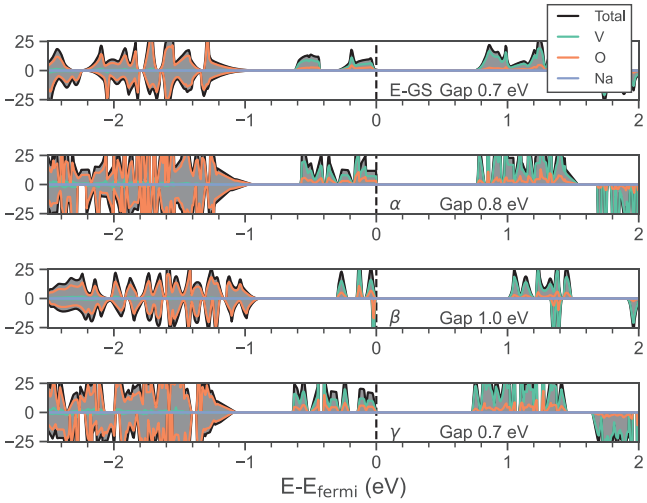

Figure S6. Computed DOS of different phases $Na_1V_2(PO_4)_3$ projected on vanadium, oxygen, and sodium atoms.

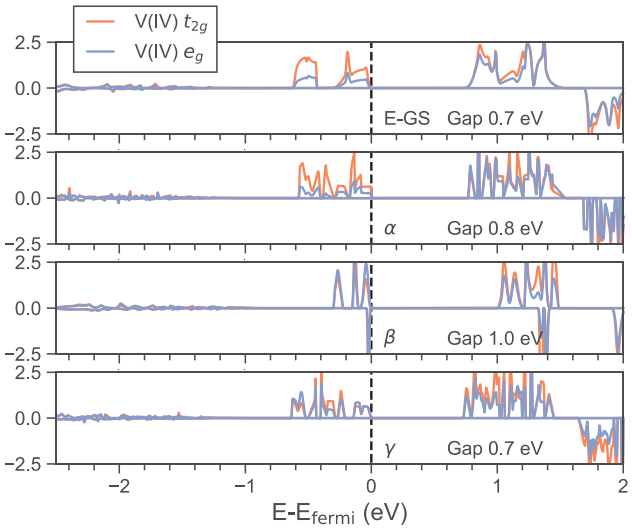

Figure S7. The computed DOS for different phases of $Na_1V_2(PO_4)_3$ projected on *3d* orbitals (i.e., t_g and e_g) of vanadium. Note that all vanadium sites within the 4 phases of $Na_1V_2(PO_4)_3$ exhibit +4 oxidation state (i.e., V(IV)).

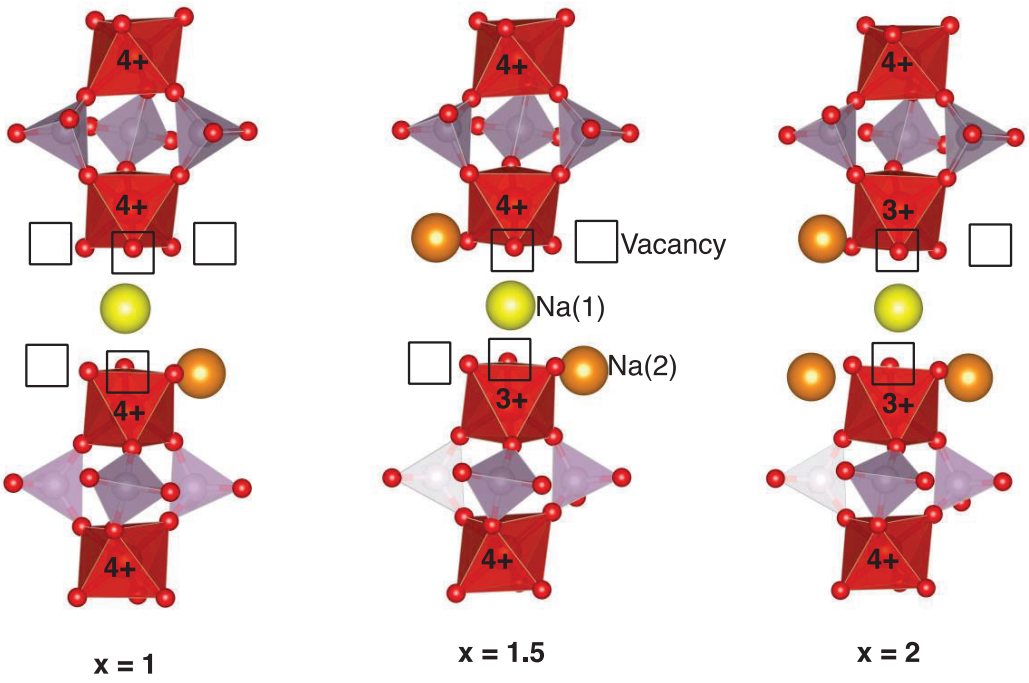

Figure S8. The local Na vacancy and vanadium charge environment of metastable phases of $Na_xV_2(PO_4)_3$, i.e., at x = 1, x = 1.5, and x = 2, corresponding to the blue phases in **Table 1** of the main manuscript. Notably, the computationally constructed structures are in the size of 2 formula units, *i.e.,* $Na_{2x}V_4(PO_4)_6$. All the $V_2(PO_4)_3$ "lantern units" are shown. Purple tetrahedra are $(PO_4)^{3-}$ polyanion groups. Charge states of vanadium sites (red octahedra) have been denoted as 3+ and 4+ for V^{3+} and V^{4+}, respectively.

The metastable phases in **Table 1** of main manuscript correspond to the computationally-predicted phases that exhibit similar Na(1)/Na(2) occupation factors with the experimentally-synthesized phases. As shown in **Figure S6**, the Na(1) site is half occupied (Na1-occ = 0.5) in all the three metastable phases. Furthermore, each Na(1) site is surrounded by 1, 2, and 3 Na(2) ions at Na compositions such as x = 1, x = 1.5, and x = 2, respectively. In addition, the occupied Na(1) sites are surrounded by vanadium sites with lower charge states. For example, at x = 1.5, the distance of Na(1)-V^{3+} is ~3.07 Å, which is shorter than ~3.12 Å for Na(1)-V^{4+}. At x = 2, the occupied Na(1) sites are closer to V^{3+} than V^{4+}, whose charges are marked

Table S1. Comparison between Rietveld refinements obtained for chemically prepared $Na_2V_2(PO_4)_3$ collected with synchrotron X-ray (black), lab X-ray with normal holder (red), lab X-ray with *in situ* cell (blue), and lab X-ray with *in situ* cell after intensity correction (green). * Note that the occupancy factors of Na(1) and Na(2) sites dramatically changed before and after the intensity correction within in-situ cell.

$Na_2V_2(PO_4)_3$

synchrotron, **standard holder**, **in-situ cell**, **in-situ cell with intensity correction**

Space group: *R*-3*c* (#167); *Z* =6

a = 8.6599(2) Å; *a* = 8.6612(3) Å;
a = 8.6506(4) Å; *a* = 8.6497(4) Å;

c = 21.8882(8) Å; *c* = 21.8903(14) Å;
c = 21.8864(14) Å; *c* = 21.8865(14) Å;

c/*a* = 2.528; *c*/*a* = 2.527;
c/*a* = 2.530; *c*/*a* = 2.530;

V = 1421.58(8) Å^3; *V*/*Z* = 236.929(13) Å^3
V = 1422.14(12) Å^3; *V*/*Z* = 237.02(2) Å^3
V = 1418.40(12) Å^3; *V*/*Z* = 236.40(2) Å^3
V = 1418.12(12) Å^3; *V*/*Z* = 236.35(2) Å^3

R_{wp} = 15.2 %; R_p = 18.1 %; R_{Bragg} = 7.46 %
R_{wp} = 22.2 %; R_p = 18.7 %; R_{Bragg} = 7.33 %
R_{wp} = 18.5 %; R_p = 34.0 %; R_{Bragg} = 8.41 %
R_{wp} = 19.9 %; R_p = 46.6 %; R_{Bragg} = 2.38 %

Atom	Wyckoff position	*x*/*a*	*y*/*b*	*z*/*c*	Uiso, Å^2	Occ.
V(1)	12c	0	0	0.1482(3) 0.1484(7) 0.1430(10) 0.1438(8)	0.012(2) 0.029(7) 0.007* 0.008*	1
P(1)	18e	0.2754(13) 0.283(3) 0.279(3) 0.279(2)	0	0.25	0.066(6) 0.109(17) 0.013* 0.040*	1
Na(1)	6b	0	0	0	0.033(14) 0.001(4) 0.013* 0.025*	0.66(4) 0.64(7) 0.94(5) 0.70(6)
Na(2)	18e	0.667(3) 0.668(5) 0.660(5) 0.643(7)	0	0.25	0.050(17) 0.05(5) 0.013* 0.035*	0.55(3) 0.57(6) 0.77(2) 0.49(2)
O(1)	36f	0.018(2) 0.018(3) 0.019(5) 0.017(6)	0.1944(17) 0.197(3) 0.198(5) 0.186(4)	0.1915(5) 0.1944(10) 0.1886(10) 0.1930(8)	0.023(6) 0.028(15) 0.051* 0.042*	1
O(2)	36f	0.1957(16) 0.193(3) 0.199(4) 0.201(3)	0.1684(16) 0.166(3) 0.175(3) 0.165(3)	0.0834(11) 0.082(2) 0.0686(17) 0.0812(18)	0.060(6) 0.104(13) 0.051* 0.070*	1

Source data tables for Figs. 1–5

Source Data Fig. 1b: X Ray powder patterns of $Na_3V_2(PO_4)_3$, $Na_1V_2(PO_4)_3$, mixtures of $Na_3V_2(PO_4)_3$ & $Na_1V_2(PO_4)_3$ at 30°C/325°C (heating)/500°C (heating)/250°C (cooling) / 35°C cooling

Source Data Fig. 1c: X Ray powder patterns of mixtures of y $Na_3V_2(PO_4)_3$ + (1-y) $Na_1V_2(PO_4)_3$ before annealing for y = 0 / 0.25 / 0.375 / 0.5 / 0.625 / 0.75 / 1

Source Data Fig. 1d: X Ray powder patterns of mixtures of y $Na_3V_2(PO_4)_3$ + (1-y) $Na_1V_2(PO_4)_3$ after annealing : $Na_1V_2(PO_4)_3$ / $Na_{1,5}V_2(PO_4)_3$ / $Na_{1,75}V_2(PO_4)_3$ / $Na_2V_2(PO_4)_3$ / $Na_{2.25}V_2(PO_4)_3$ / $Na_{2.5}V_2(PO_4)_3$ / $Na_3V_2(PO_4)_3$

Source Data Fig. 2a: X Ray powder pattern of e-$Na_2V_2(PO_4)_3$

Source Data Fig. 3a: Galvanostatic curve of e-$Na_2V_2(PO_4)_3$ & c-$Na_2V_2(PO_4)_3$ between 2.5 and 4.25 V vs Na^+/Na

Source Data Fig. 3d: GITT curve of c-$Na_2V_2(PO_4)_3$

Source Data Fig. 3f: Galvanostatic curve of c-$Na_2V_2(PO_4)_3$ between 3 and 0.5 V vs Na^+/Na

Source Data Fig. 4a: X ray powder patterns from operando measurements in the 2.5–4.4 V region

Source Data Fig. 4b: X ray powder patterns from operando measurements in the 1.3–3 V region

Source Data Fig. 5: X ray diffraction patterns of $V_2(PO_4)_3$ chemically deintercalated and $Na_{0.5}V_2(PO_4)_3$ charged at 4.4 V